UNIVERSITY OF AMSTERDAM

UvA-DARE (Digital Academic Repository)

Efficient Separation of Ethanol-Methanol and Ethanol-Water Mixtures Using ZIF-8 Supported on a Hierarchical Porous Mixed-Oxide Substrate

Tang, Y.; Dubbeldam, D.; Guo, X.; Rothenberg, G.; Tanase, S.

DOI
10.1021/acsami.9b02325

Publication date
2019

Document Version
Final published version

Published in
ACS Applied Materials and Interfaces

License
CC BY-NC-ND

Link to publication

Citation for published version (APA):
Tang, Y., Dubbeldam, D., Guo, X., Rothenberg, G., & Tanase, S. (2019). Efficient Separation of Ethanol-Methanol and Ethanol-Water Mixtures Using ZIF-8 Supported on a Hierarchical Porous Mixed-Oxide Substrate. *ACS Applied Materials and Interfaces*, *11*(23), 21126-21136. https://doi.org/10.1021/acsami.9b02325

General rights
It is not permitted to download or to forward/distribute the text or part of it without the consent of the author(s) and/or copyright holder(s), other than for strictly personal, individual use, unless the work is under an open content license (like Creative Commons).

Disclaimer/Complaints regulations
If you believe that digital publication of certain material infringes any of your rights or (privacy) interests, please let the Library know, stating your reasons. In case of a legitimate complaint, the Library will make the material inaccessible and/or remove it from the website. Please Ask the Library: https://uba.uva.nl/en/contact, or a letter to: Library of the University of Amsterdam, Secretariat, Singel 425, 1012 WP Amsterdam, The Netherlands. You will be contacted as soon as possible.

UvA-DARE is a service provided by the library of the University of Amsterdam (https://dare.uva.nl)

Download date:28 Aug 2022

This is an open access article published under a Creative Commons Non-Commercial No Derivative Works (CC-BY-NC-ND) Attribution License, which permits copying and redistribution of the article, and creation of adaptations, all for non-commercial purposes.

ACS APPLIED MATERIALS & INTERFACES

Research Article

Cite This: ACS Appl. Mater. Interfaces 2019, 11, 21126−21136

www.acsami.org

Efficient Separation of Ethanol−Methanol and Ethanol−Water Mixtures Using ZIF-8 Supported on a Hierarchical Porous Mixed-Oxide Substrate

Yiwen Tang,[†] David Dubbeldam,[†] Xingmei Guo,[‡] Gadi Rothenberg,[†] and Stefania Tanase*[,†]

[†]Van't Hoff Institute for Molecular Sciences, University of Amsterdam, Science Park 904, 1098 XH Amsterdam, The Netherlands

[‡]School of Environmental and Chemical Engineering, Jiangsu University of Science and Technology, No. 2 Mengxi Road, Zhenjiang 212003, Jiangsu, China

Supporting Information

ABSTRACT: This work reports a new approach for the synthesis of a zeolitic imidazolate framework (ZIF-8) composite. It employs the direct growth of the crystalline ZIF-8 on a mixed-metal oxide support TiO_2−SiO_2 (TSO), which mimics the porous structure of *Populus nigra*. Using the natural leaf as a template, the TSO support was prepared using a sol−gel method. The growth of the ZIF-8 layer on the TSO support was carried out by the *seeds and second growth* method. This method facilitates the homogeneous dispersion of ZIF-8 crystals at the surface of the TSO composite. The ZIF-8@TSO composite adsorbs methanol selectively, mainly due to the hierarchical porous structure of the mixed oxide support. As compared with the as-synthesized ZIF-8, a 50% methanol uptake is achieved in the ZIF-8@TSO composite, with only 25 wt % ZIF-8 loading. IAST simulations show that the ZIF-8@TSO composite has a preferential adsorption toward methanol when using an equimolar methanol−ethanol mixture. An opposite behavior is observed for the as-synthesized ZIF-8. The results show that combining MOFs and mixed-oxide supports with bioinspired structures opens opportunities for synthesizing new materials with unique and enhanced adsorption and separation properties.

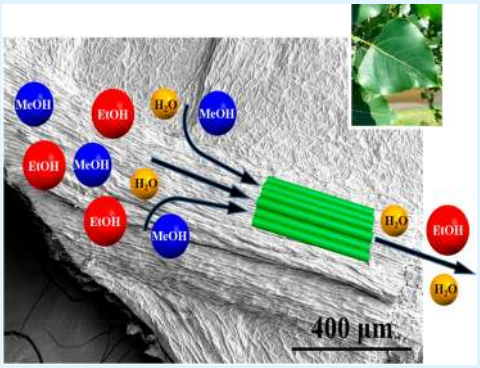

KEYWORDS: *ZIF-8, artificial leaf, hierarchical system, composite, adsorption*

1. INTRODUCTION

Developing porous materials with selective molecular adsorption properties is highly relevant for molecular storage and separation.[1−3] Such materials enable more efficient industrial processes[4,5] and facilitate the production of clean energy.[6,7] They are also used in environmental protection[8] and air quality monitoring.[9] Metal−organic frameworks (MOFs) are a specific class of porous materials, consisting of metal ions linked together by polydentate organic linkers.[10] These materials are foreseen as ideal candidates for molecular storage and separation because of their large internal surface area and tunable porous structure.[5,11−14] MOFs are commonly synthesized using conventional hydrothermal or solvothermal synthetic methods, which often yield powders of tiny crystals.[15] Such powders cannot be directly used because they have limited packing densities and high diffusion barriers. This limits the practical applications of MOFs due to increased risk of contamination or even blocking of industrial pipelines.[15] Some studies indicate that these downsides can be overcome by shaping the MOF powders as granules, pellets, or monoliths[16−18] or by dispersing them within thin films, creating membranes.[19−21] The main drawback associated with such shaping methods is the loss of crystallinity due to the applied pressure, leading to the inactivation of the material.[15] As for the MOFs-based membrane, there is usually a pressure drop of the mixture stream over the membrane after its permeation, leading to lower fluxes.[22] Therefore, finding the most appropriate processing method of MOFs is still a big challenge.

To tackle the above-mentioned challenges, we turned our attention to Mother Nature. Plant leaves have attracted our interest due to their natural hierarchical porous system which consists of many fibers and vessels of different sizes. Hierarchically porous materials often present decreased diffusion barriers and enhanced adsorption performance compared to uniformly sized porous materials.[1] Therefore, we aimed at designing a new MOF-based composite which has a hierarchical porous structure, replicated from a natural leaf. We hypothesized that growing crystalline MOFs at the surface of an artificial leaf support would yield a material that combines the macropores and mesopores of the artificial leaf with the micropores of MOFs in a hierarchical porous structure. Furthermore, the fine-tuning of the interactions

Received: February 8, 2019
Accepted: May 20, 2019
Published: May 22, 2019

Downloaded via UNIV AMSTERDAM on August 13, 2019 at 07:05:34 (UTC).
See https://pubs.acs.org/sharingguidelines for options on how to legitimately share published articles.

© 2019 American Chemical Society

DOI: 10.1021/acsami.9b02325
ACS Appl. Mater. Interfaces 2019, 11, 21126−21136

between the MOF crystals and the surface of the support may prevent the agglomeration of the former.

Populus nigra, a tree that grows throughout northern Europe, was used as a template to prepare a porous mixed-oxide support. It is known that Ti^{2+} ions substitute the Mg^{2+} ions within the porphyrins of the chlorophyll molecules of the plants[23] and that TiO_2 is used to make porous ultrafiltration membranes for dye-water separations.[24] Therefore, we selected TiO_2 as the most appropriate material to replicate the vein structure of the natural *Populus nigra* leaves. To prevent the collapse of the primary vein structure of the leaf and to compensate the partial loss of the delicate original nature leaf's structure during the replication process, we added SiO_2 as a structure stabilizer and Pluronic P123 as a mesoporous template.[25]

The natural leaf vein system evolved for transporting aqueous liquids. Therefore, we focused our study on liquid adsorption and separation. Bioethanol is an environmentally benign and renewable source of energy which is directly produced from agricultural feedstocks. The raw product contains water and other organic alcohols as byproducts,[26] and therefore, bioethanol must be purified before it can be used as fuel.[27] A few MOFs, including MIL-53 (Cr),[28] JUC-110,[29] Ce(BTB)(H_2O),[30] and Cu(mtpm)Cl_2[31] were studied as adsorbents for water−alcohol and alcohol−alcohol adsorption and separation processes. However, these materials also have a low stability in the presence of water. Our study focused on the zeolitic imidazolate framework 8 (ZIF-8), which is known as one of the most chemically and thermally stable MOFs with a very good stability in water.[32] ZIF-8 has different adsorption properties in the presence of water, methanol, and ethanol as a result of its hydrophobic structure.[33] Therefore, we use it to prepare a composite material by growing ZIF-8 crystals at the surface of a TiO_2−SiO_2 support which replicates the natural leaf structure. The adsorption properties of this new MOF composite toward ethanol, methanol, and water were measured experimentally. The ideal adsorbed solution theory (IAST) method was used to predict the water−ethanol and methanol−ethanol separation properties of the composite material. There are a few MOF mixed matrix membranes demonstrating the efficient separation of water−alcohol mixtures.[34−39] However, these studies also show that the separation performance is influenced significantly by the mass swelling degree of the membranes.[34,36−39] To the best of our knowledge, this is the first MOF-based composite applied in water−alcohol separation using a robust mixed-oxide structure as support.

2. EXPERIMENTAL SECTION

2.1. Materials. Zinc nitrate hexahydrate (≥99% purity), 2-methylimidazolate (Hmim, 99% purity), dipotassium phosphate (≥98% purity), 1-methylimidazole (96% purity), potassium dihydrogen phosphate (≥99% purity), glutaraldehyde solution (25% in H_2O), titanium(IV) isopropoxide (TIPO, ≥97% purity), tetraethylorthosilicate (TEOS, 98% purity), Pluronic P123, and poly(styrenesulfonate) sodium salt (PSS) were purchased from Aldrich Chemical Co. Unless noted otherwise, all chemicals were used without further purification.

2.2. Physical Methods. Powder X-ray diffraction (PXRD) measurements were carried out on a Rigaku Miniflex X-ray diffractometer. PXRD measurements were carried out in the 5−50° range using a Cu−Kα source. Infrared spectra (IR, 4000−400 cm^{-1}, resol. 0.5 cm^{-1}) were recorded on a Varian 660 FTIR spectrometer equipped with a Gladi ATR device using KBr pellets. Raman spectra were recorded using an Olympus BX51 M upright microscope with excitation at 632.8 nm (Thorlabs HNL 120-1 HeNe laser) via a 50× magnification objective with 10 mW at sample. Raman scattering was collected and delivered to a Shamrock163 spectrograph via a round to line fiber bundle and detected with an iDus-416 CCD detector. Thermogravimetric analysis (TGA) and differential scanning calorimetry (DSC) measurements were carried out on a NETZSCH STA 449 F3 Jupiter Instrument. The morphology of the samples with sputtered gold was studied by using Scanning Electron Microscopy (SEM, FEI Verios 460 scanning electron microscope) operated at 5 kV, and the affiliated SEM-EDS was used to analyze the composition of the samples. Morphological analysis was performed by using Transmission Electron Microscopy and High Resolution Transmission Electron Microscopy (TEM/HRTEM; JEM 2010 HT). X-ray photoelectron spectroscopy (XPS) measurements were done using an AXIS Ultra instrument with monochromatized Al Kα excitation. Electromagnetic paramagnetic resonance (EPR) spectra were recorded at 77 K on a Bruker EMX X-band spectrometer equipped with a helium cryostat and using a center field at 3000.00 G, a modulation amplitude of 4.000 G, a microwave frequency of 9.392 GHz, and a power of 0.6325 mW. Samples were measured under nitrogen. Nitrogen adsorption isotherms were measured on a Thermo Scientific Surfer instrument at 77 K. Water, methanol, and ethanol adsorption isotherms were measured on a microcalorimeter (Calvet C80, Setaram) which can operate isothermally, and it is connected to a home-built manometric apparatus at 303 K.[40] Before each adsorption measurement, samples were outgassed overnight at 473 K under vacuum (<10^{-4} Torr).

2.3. Synthesis of ZIF-8. Crystalline ZIF-8 samples were prepared using a modification of a published procedure.[31] First, 734.4 mg (2.5 mmol) of $Zn(NO_3)_2{\cdot}6H_2O$ was dissolved in 50 mL of methanol. In a second flask, 810.6 mg (10 mmol) of Hmim and 810.6 mg (10 mmol) of 1-methylimidazole were dissolved in 50 mL of methanol. The latter solution was poured slowly into the former clear solution under vigorous stirring. After 24 h aging without stirring, the white precipitate was collected by filtration, washed with fresh methanol, and dried overnight under ambient conditions.

2.4. Synthesis of the Artificial Leaf Support TSO (T, S, and O Refer to Titanium, Silicon, and Oxygen, Respectively). The TSO support was synthesized via a modified published procedure.[26,41] Fresh *Populus nigra* leaves were treated overnight with a 2.5% glutaraldehyde-phosphate buffered saline (PBS, pH = 7.2) solution at 277 K. This step is required for the fixation of the plant's tissues. The prefixed leaves were rinsed in the buffer solution with a solution having the same concentration that was used in the previous step and then underwent a graded dehydration process, in which the leaves were immersed stepwise into ethanol solutions with concentrations of 10%, 20%, 30%, 50%, and 80% for 20 min, respectively. Then, the leaves were immersed in a 5 wt % diluted HCl solution for 3 h to remove the Mg^{2+}, K^+, and Ca^{2+} ions.

The TSO precursor solution was prepared by dissolving 1.5 g of P123, which works as a mesoporous template, in 1.8 g of concentrated HCl. The resulting mixture was added to 40 mL of preheated (40 °C) ethanol and stirred for 3 h. Then, 2.34 g (8 mmol) of TIPO and 0.43 g (2 mmol) of TEOS were added, and the resulting mixture was stirred vigorously for another 4 h. The pretreated leaves were then soaked in this precursor solution overnight and then washed with deionized water (3 × 20 mL). The infiltrated leaves were dried at 353 K for 6 h and then calcined in air at 873 K for 4 h to remove the organic materials and promote the crystallization of the mixed TiO_2−SiO_2 oxide.

2.5. Synthesis of the ZIF-8@TSO Composite Material. A well-dispersed ZIF-8 methanol suspension (0.2 wt %) was first prepared by sonicating ZIF-8 in 50 mL of methanol. Separately, the presynthesized TSO was dispersed in 50 mL of aqueous PSS (15.0 wt % solution) at room temperature for 2 h. The TSO sample was then washed with distilled water (3 × 20 mL) and then added to the ZIF-8 suspension. This mixture was aged overnight at room temperature, filtered, and then dried in air under ambient conditions, giving a TSO coated with a layer of ZIF-8 seeds. The solid material obtained was then added into a second ZIF-8 solution to grow the ZIF-8 layer. The second

DOI: 10.1021/acsami.9b02325
ACS Appl. Mater. Interfaces 2019, 11, 21126−21136

ZIF-8 solution was prepared from 1 g (12 mmol) of 2-methylimidazole and 0.055 g (0.2 mmol) of $Zn(NO_3)_2{\cdot}6H_2O$ dissolved in 20 mL of methanol. The coated TSO was added to this solution and then aged in an oven at 333 K for 6 h, forming the second layer of ZIF-8. Finally, the resulting composite material, designated ZIF-8@TSO, was washed with 10 mL of methanol and dried in air under ambient conditions.

3. RESULTS AND DISCUSSION

3.1. Materials Synthesis and Characterization. Scheme 1 summarizes the synthetic procedure for the synthesis of the ZIF-8@TSO composite. The mixed-oxide support was synthesized using a modified reported procedure[26,41] and functionalized with PSS to achieve a negatively charged surface that facilitates the binding of Zn^{2+} at the surface of the support.[48,49] Then, the ZIF-8 crystals were grown at the surface of TSO using a seeding and second growth method. Combining a microporous ZIF-8 layer with the meso/macroporous features of the TSO support enables obtaining a composite material, ZIF-8@TSO, with a hierarchical pore structure. Due to the presence of the hydrophobic ZIF-8 layer on the surface of the ZIF-8@TSO composite, we hypothesized that the composite will selectively adsorb methanol and ethanol from water−alcohol mixtures (see Scheme 2). Before studying the adsorption properties of the ZIF-8@TSO composite, all materials were characterized using a combination of spectroscopic and surface characterization techniques.

Scheme 1. Coating of a Crystalline ZIF-8 Layer on a TiO_2−SiO_2 (TSO) Support Creates a Composite Material That Combines the Advantages of Selective Adsorption of ZIF-8 with the Hierarchical Channel Structure of the Support

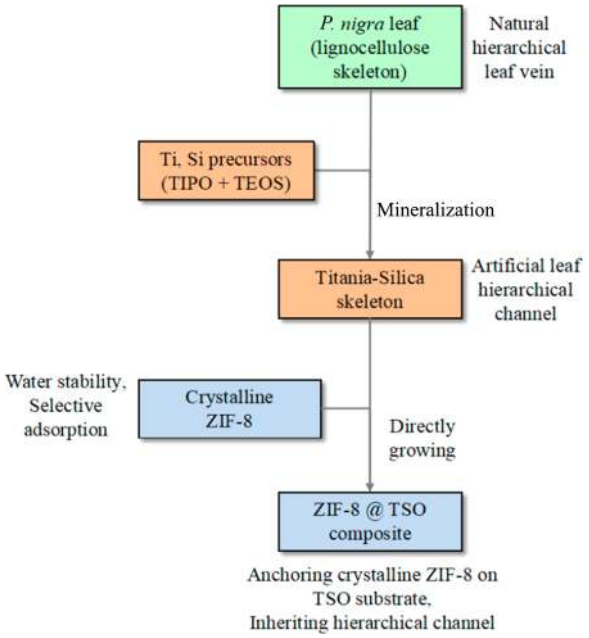

The TSO support was characterized using several techniques, including Powder X-ray Diffraction (PXRD), High Resolution Transmission Electron Microscopy (HRTEM), Scanning Electronic Microscopy (SEM), EDS elemental analysis, and X-ray Photoelectron Spectroscopy (XPS). Figure 1a reveals that the TiO_2 phase within the TSO crystallizes in the tetragonal anatase structure.[42] Based on the HRTEM (see Figure 1b), the lattice spacing of 0.35 nm is assigned to the (101) plane of anatase TiO_2.[43] This is in excellent agreement with the PXRD data (see Figure 1a). The SiO_2 phase within TSO support is present in amorphous form and encircles the randomly distributed crystalline TiO_2 particles (see Figure S1 in the SI). Scanning electron microscopy (SEM) was performed to shed light on the morphology of the TSO support. Figure

Figure 1c clearly shows the macroscale channels on the cross section of the TSO support, indicating that the vein structure of the natural leaf is replicated. As shown in Figure 1d, the replicated channels run along the entire artificial leaf without breaking. The windows on the channels of the TSO support are also observed (see Scheme 1 and Figure S2 in the SI).

Further analysis of the TSO support by EDS elemental mapping confirms the presence of Ti, Si, and O (see Figure 1e and Figure S3). In addition, the XPS spectra were recorded to characterize the elemental state of the TSO surface. As shown in Figure 2a, the Ti 2*p* XPS spectrum shows four components with binding energies at 458.7 and 464.5 eV corresponding to the Ti^{4+} ions and at 457.5 and 463.1 eV assigned to Ti^{3+} ions.[44] The O 1*s* XPS spectrum has three components at binding

Scheme 2. Schematic Illustration of the ZIF-8@TSO Composite Formed by Growing Dodecahedra ZIF-8 Crystals at the Surface of the TSO Support[a]

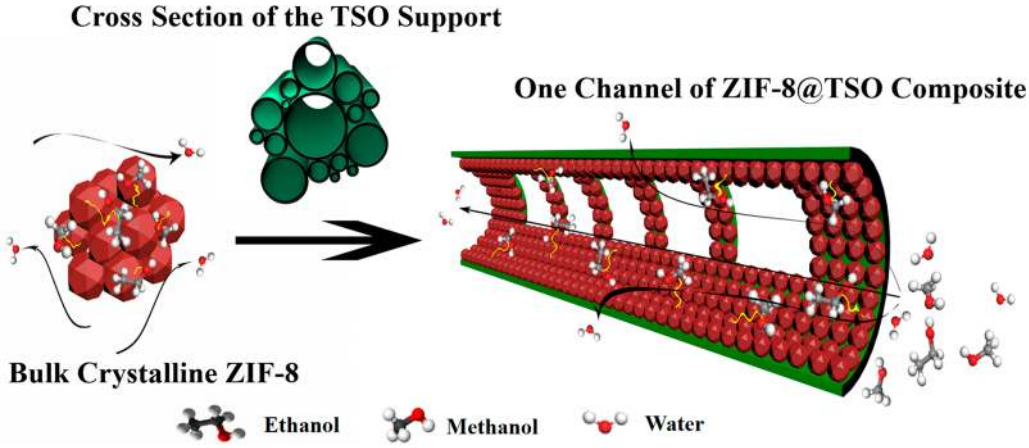

[a]The ZIF-8 crystals are arranged along the channels of the TSO support and work as a selective adsorption core.

DOI: 10.1021/acsami.9b02325
ACS Appl. Mater. Interfaces 2019, 11, 21126−21136

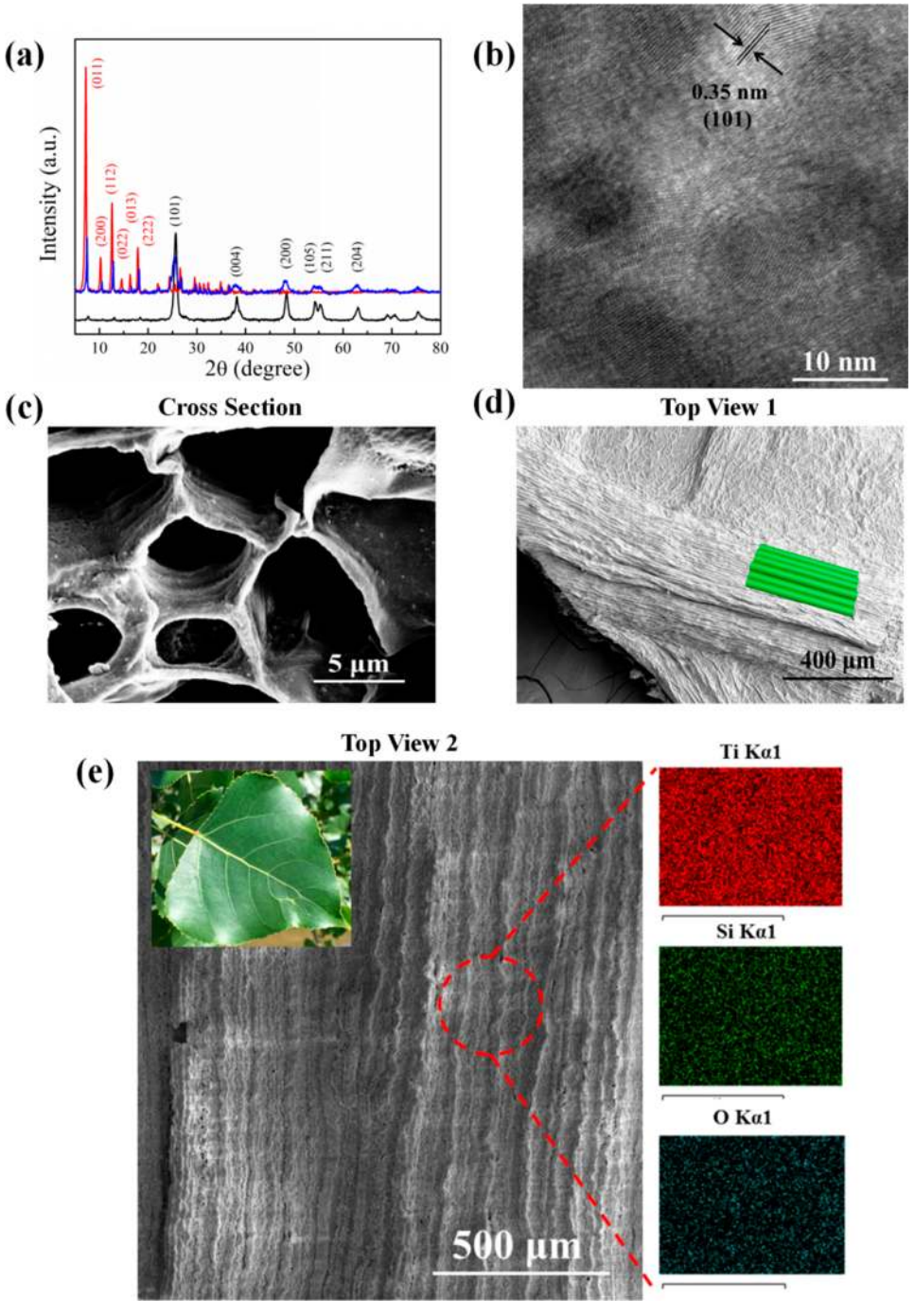

Figure 1. (a) PXRD patterns of the TSO support (black), the bulk crystalline ZIF-8 (red), and the ZIF-8@TSO composite (blue). (b) HRTEM image of the TSO support. (c) Micrograph photo showing the cross section of the channel architecture in the TSO support. (d) The top view of the TSO support, with the inset as the schematic illustration to show the tubes. (e) EDS elemental mapping of the TSO support leaf corresponding to the red circle, with the inset as the optical image of the *Populus nigra* leaf; the EDS scale bars are 10 μm.

energies of 529.9, 531.3, and 532.2 eV corresponding to the bonds of Ti−O, Si−O−Ti, and Si−O, respectively (Figure 2b). Similar to the Ti 2*p* spectrum, the Si 2*p* XPS spectrum has two components (Figure 2c). The bands at 103.5 and 102.5 eV can be assigned to Si^{4+} and Si^{3+} ions, respectively.[45] The XPS analysis indicates the presence of Ti^{3+} and Si^{3+} on the surface of the TSO to form TiO_{2-x} and SiO_{1-x}, thus revealing that the surface of TSO is not stoichiometric and has some oxygen vacancies. Furthermore, the XPS results also indicate the formation of the TiO_2−SiO_2 mixed-oxide at the surface, in agreement with the HRTEM studies (see Figure S1 in the SI). Both the existence of oxygen vacancies and Ti^{3+} ions in the TSO artificial leaf was further confirmed by electron paramagnetic resonance (EPR) studies. A sharp signal at g = 2.00 is observed, indicating the presence of oxygen vacancies (see Figure 2d).[46] The broad and anisotropic signal with a g value of 1.98 is due to the presence of paramagnetic Ti^{3+} ions (see Figure 2d).[47] Similar spectroscopic features are also observed for the ZIF-8@TSO composite (see Figure 2d).

The ZIF-8@TSO composite was characterized by PXRD, FTIR, Raman, SEM, EPR and EDS elemental analysis. The IR spectrum of TSO modified with PPS (see Figure S4 in the SI)

DOI: 10.1021/acsami.9b02325
ACS Appl. Mater. Interfaces 2019, 11, 21126−21136

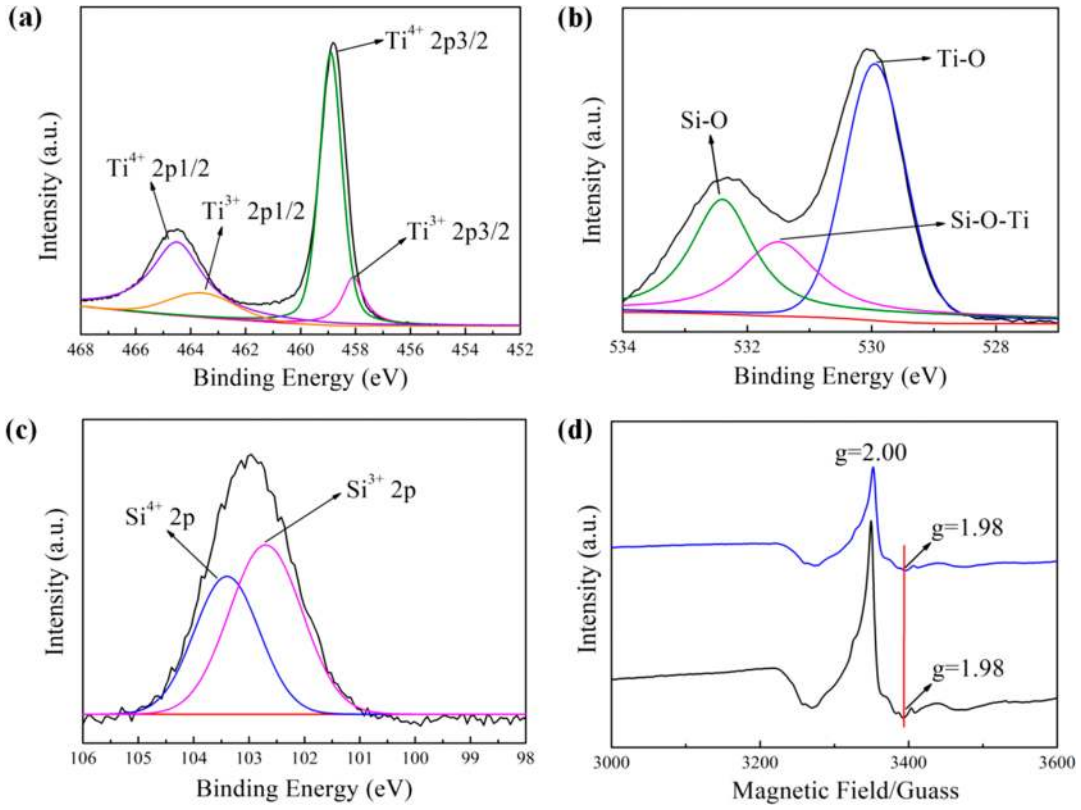

Figure 2. (a) Ti 2*p*, (b) O 1*s*, and (c) Si 2*p* XPS spectra of the TSO support, respectively, and (d) the EPR spectra of the TSO support (black) and ZIF-8@TSO composite (blue).

presents the characteristic peaks of PSS chains,[48] indicating that PSS was indeed grafted on the TSO surface. Figure 1a shows that the PXRD pattern of the ZIF-8@TSO composite contains the characteristic peaks of both crystalline ZIF-8 and TSO support, confirming the presence of both ZIF-8 and TSO. Figure 3a shows the FTIR spectra of the TSO support, as-synthesized ZIF-8, and ZIF-8@TSO composite. Compared to TSO, the IR spectrum of ZIF-8@TSO presents not only the Ti−O−Ti, Ti−O−Si, and Si−O−Si stretching vibrations (at 500, 970, and 1100 cm^{-1}) but also the additional vibration bands which are characteristic to the ZIF-8.[50] For instance, the band at 421 cm^{-1} is assigned to the Zn−N stretching, while the bands in the 500−1350 cm^{-1} and 1350−1500 cm^{-1} ranges are assigned to the in- and out-of-plane bending and stretching of the C−H bonds of the imidazole ring, respectively. The C═N (aromatic) stretching vibrations at around 1548 cm^{-1} and the aliphatic C−H stretching vibrations at 2929 and 3135 cm^{-1} are all characteristic to the ZIF-8 material.[51,52] Furthermore, a broad peak at around 3200 cm^{-1} in both TSO and ZIF-8@TSO corresponds to the surface silanol (Si−OH) groups.[53] The Raman spectra of ZIF-8 and ZIF-8@TSO also confirm that the composite contains ZIF-8 (see Figure 3b), the bands at 687 cm^{-1} and in the range 1000−1600 cm^{-1} being assigned to the imidazole ring puckering, C5−N stretching, C−H wagging, and C4−C5 stretching modes, respectively.[54] The bands at 2931, 3114, and 3131 cm^{-1} respectively correspond to the $C-H_{methyl}$ and $C-H_{arom}$ stretching modes.[55] These results, together with the FTIR results, confirm that both the ZIF-8 crystals and TSO artificial leaf support are present in the ZIF-8@TSO composite.

The morphology of the ZIF-8@TSO composite was further characterized by SEM (Figure 4). The as-synthesized ZIF-8 crystals have a dodecahedral shape and a narrow size distribution (ca. 400 nm, see Figure 4a), facilitated by the modulating ligand 1-methylimidazole. Figure 4b displays a top view of the ZIF-8@TSO composite indicating the replicated channels. The cross section of ZIF-8@TSO channels which are larger than 3 μm is shown in Figure 4c. Figure 4c also shows that the ZIF-8 crystals are almost homogeneously dispersed on the surface of the TSO support. As discussed above, PSS acts as linker enabling the growth of ZIF-8 crystals on TSO surface. Moreover, the functionalization of the TSO surface with PSS enables the homogeneous dispersion of the ZIF-8 crystals. Using nonfunctionalized TSO leads to only several ZIF-8 crystals randomly dispersed on the TSO surface (see Figure S5 in the SI). EDS analysis (Figure 4d) reveals that the surface elementary composition of the ZIF-8@TSO is similar to that of as-synthesized ZIF-8 (see also Figure S6 in the SI), with Ti and Si from the TSO also present. Consequently, the combined FTIR, Raman, SEM, and EDS elemental analysis demonstrate that the ZIF-8 crystals were successfully and homogeneously grown on the TSO artificial leaf surface.

Figure 5 displays the thermogravimetric analysis (TGA) and differential scanning calorimetry (DSC) data, showing that all the organic matter derived from the natural leaf is completely removed above 873 K. The decomposition of the ZIF-8@TSO composite occurs above 673 K, which is much higher than the decomposition temperature of the Hmim ligand yet similar to that of bulk crystalline ZIF-8. This indicates that the first mass loss is due to the decomposition of the ZIF-8 crystal layer. The first weight loss observed in the TGA of the ZIF-8@TSO composite corresponds to a loading of 25 wt % of ZIF-8 on the TSO surface.

DOI: 10.1021/acsami.9b02325
ACS Appl. Mater. Interfaces 2019, 11, 21126−21136

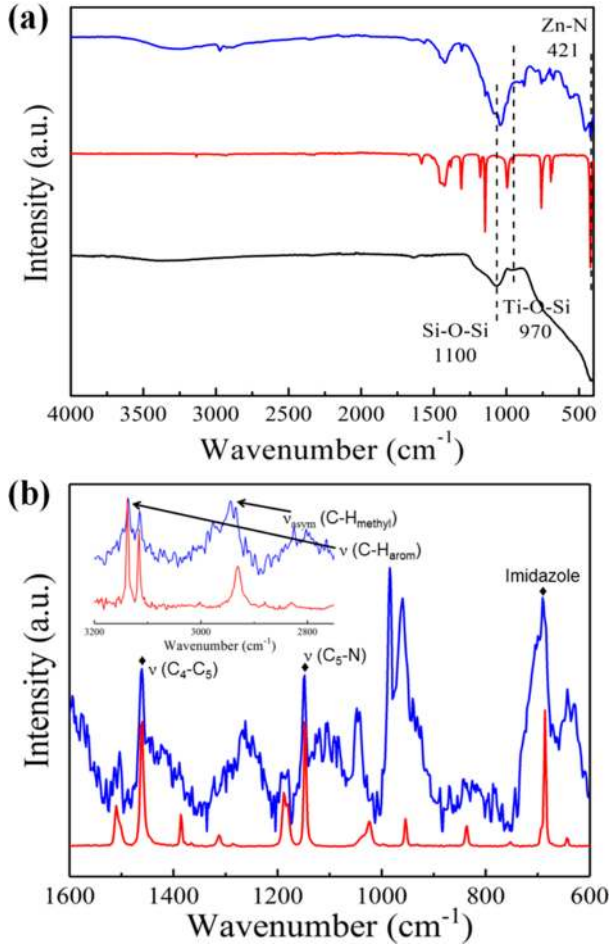

Figure 3. (a) FTIR spectra of the TSO (black), ZIF-8 (red), and the ZIF-8@TSO composite (blue). (b) Raman spectra (λ_{exc} = 632.8 nm) of the ZIF-8 and the ZIF-8@TSO composite.

3.2. Adsorption Studies. Nitrogen adsorption−desorption studies were carried out to characterize the porous structure and the surface area of the TSO support, the as-synthesized ZIF-8, and the ZIF-8@TSO composite, respectively. The TSO support displays a type IV isotherm with a desorption hysteresis, indicating a mesoporous material (see Figure 6). The presence of mesopores is additionally confirmed by TEM (see Figure S7 in the SI), wherein wormlike mesopores are observed. Using the Barrett−Joyner−Halenda (BJH) method, a mesopore size distribution of ca. 3−20 nm and a mesopore volume of 0.49 cm^3/g are determined. Moreover, compared to the mesopores, negligible micropores with the average pore size of ca. 1.3 nm and a volume of 0.08 cm^3/g (calculated by the Saito and Foley method) can be observed within TSO. The Brunauer−Emmett−Teller (BET) and Langmuir surface areas are about 180 and 190 m^2/g, respectively (see Table 1). The surface area of TSO support is much higher than that of the traditional TiO_2 materials, e.g., P25 with a surface area of 50 m^2/g.[55]

Unlike the TSO, the bulk crystalline ZIF-8 shows a type I isotherm, suggesting that it is microporous. In agreement with earlier reports,[33] the bulk crystalline ZIF-8 has an average micropore size of ca. 1.2 nm and a pore volume of 0.69 cm^3/g, respectively. The determined BET and Langmuir surface areas of 1720 and 1800 m^2/g (see Table 1) are also in agreement with previous studies.[33] A few mesopores of ca. 4 nm with a pore volume of 0.05 cm^3/g are present, most likely due to the interparticle void of ZIF-8 crystals.

The ZIF-8@TSO composite has a H3-type type I isotherm, which can be attributed to a hierarchical porous structure (see Figure 6). The micropores have a diameter of ca. 1.2 nm, similar to that found for the bulk crystalline ZIF-8, indicating that they belong to the ZIF-8 layer. The micropore volume is 0.25 cm^3/g. A mesopore size distribution of ca. 4−10 nm with a mesopore volume of 0.10 cm^3/g is calculated, indicating that some large mesopores within TSO support were blocked by the ZIF-8 crystals. The BET and Langmuir surface areas of the ZIF-8@TSO composite are 400 and 530 m^2/g, respectively (see Table 1). Taking into consideration that the ZIF-8 crystals account for 25 wt % in the ZIF-8@TSO composite, the surface area for the composite is relatively high. This is because the functionalized TSO support prevents the aggregation of the ZIF-8 crystals and favors their good dispersion at the TSO surface, thereby increasing the accessibility of ZIF-8 for nitrogen molecules. Furthermore, it is likely that some interstitial voids are formed between the ZIF-8 crystals and the TSO support, increasing the observed surface area for the composite.[56]

The water, methanol, and ethanol adsorption properties of ZIF-8, TSO support, and ZIF-8@TSO composite were studied separately at 303 K (see Figure 7). ZIF-8 has a type III isotherm with a very low water uptake (<0.1 mmol/g) even at the saturation pressure. The type III isotherm reveals a low interaction between the adsorbate and the adsorbent, which is in agreement with the presence of the hydrophobic 2-methylimidazolate linkers in the ZIF-8 framework.[57] A higher water uptake is observed for the TSO support and the ZIF-8@TSO composite, although their surface areas are much lower than that of the ZIF-8 (see Figure 7a). This is due to the presence of the surface bridging oxygen atoms of the TiO_2 phase as well as the silanol (Si−OH) groups of the SiO_2 phase of the TSO. Both are effective adsorption sites that can form hydrogen bonds with the water molecules.[58,59]

In agreement with earlier studies,[60] the ethanol and methanol uptakes are much higher than the water uptake in the case of ZIF-8. The isotherms are of S-shaped type V, indicating the presence of weakly interacting adsorbates in a microporous adsorbent. Figure 7b shows that the methanol adsorption is weak at low pressures due to the hydrophobic surface of the ZIF-8. Above $P/P^0 \approx 0.2$, however, the adsorption increases sharply as a consequence of continuous pore filling. Initially, a few adsorbed methanol molecules form small clusters, which exert attractions for the following adsorbed methanol molecules and then grow into a three-dimensional network filling the pores. This is the so-called cluster-formation and cage-filling process.[61] A continuous pore filling is also observed in the adsorption of ethanol. However, a shorter initial adsorption plateau is observed at low pressures, indicating that in ZIF-8 the ethanol adsorption is higher than that of methanol at low pressures (see Figure 7c). This is because the hydrophobic ZIF-8 has a stronger affinity for the less polar ethanol molecules (relative polarity 0.654) as compared with methanol (relative polarity 0.762). The molecular adsorption is mainly controlled by entropic factors at high pressures. Thus, a higher saturation capacity is observed for methanol (kinetic diameter is 3.6 Å) than ethanol (kinetic diameter is 4.3 Å).[62]

As compared with ZIF-8, the TSO support has a very different methanol adsorption behavior (see Figure 7b). Based

DOI: 10.1021/acsami.9b02325
ACS Appl. Mater. Interfaces 2019, 11, 21126−21136

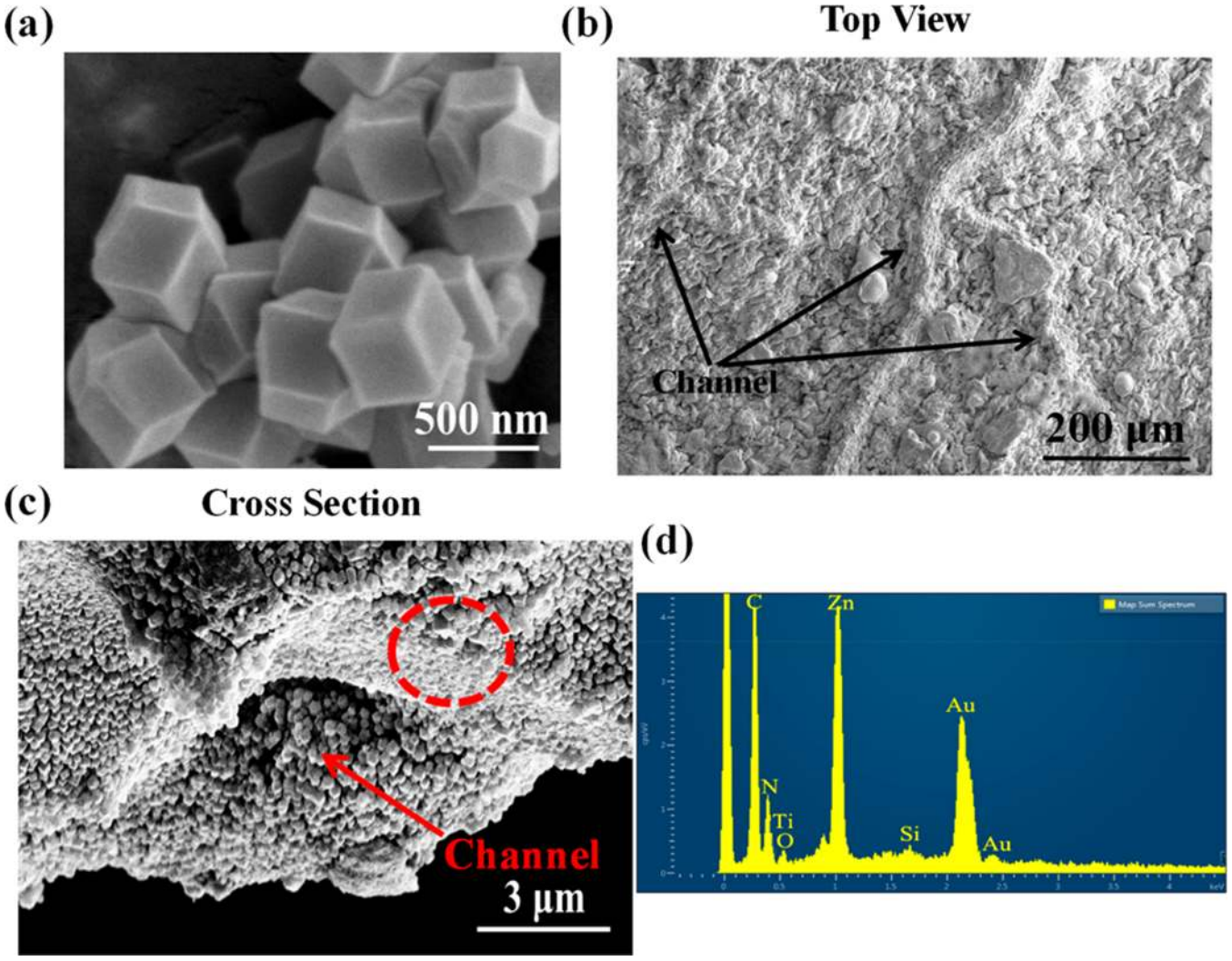

Figure 4. (a) SEM image of the as-synthesized rhombic dodecahedra ZIF-8 crystals. (b) Top view of the ZIF-8@TSO composite, with the black arrow indicating the channels of the artificial leaf. (c) Cross section view of the ZIF-8@TSO composite, with the red arrow indicating the opening gate of the artificial leaf channel. (d) EDS spectrum of the ZIF-8@TSO composite corresponding to the red circle in part (c).

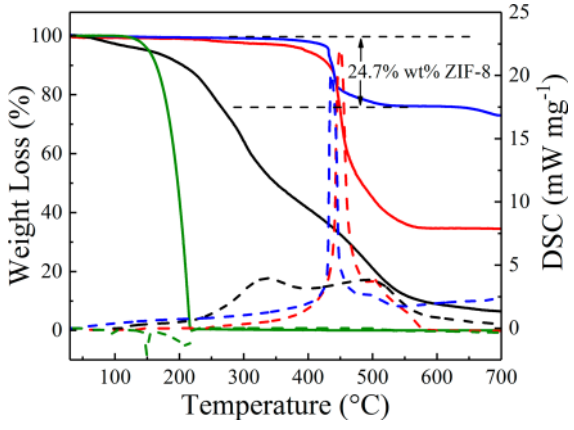

Figure 5. TGA (solid lines) and DSC (dashed lines) curves of the ZIF-8@TSO composite (blue), the as-synthesized ZIF-8 (red), the dehydrated natural leaf (black), and the Hmim ligands (dark green) measured under air at a heating rate of 5 °C/min.

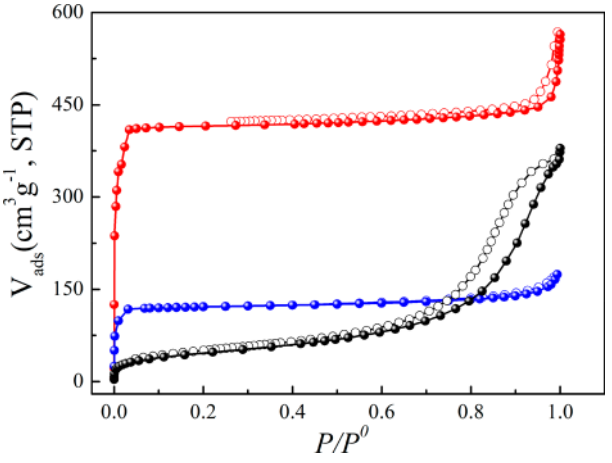

Figure 6. N_2 adsorption isotherms measured at 77 K of the as-synthesized ZIF-8 (red), the TSO artificial leaf (black), and the ZIF-8@TSO composite (blue).

on the characterization studies above, the TSO support contains two phases: the anatase TiO_2 with oxygen point defects and amorphous SiO_2. The silanol groups on the silica surface can form hydrogen bonds with the methanol and ethanol molecules. However, the dissociative adsorption of methanol is favored over molecular adsorption at low pressure

DOI: 10.1021/acsami.9b02325
ACS Appl. Mater. Interfaces 2019, 11, 21126−21136

Table 1. Physical Properties of the as-Synthesised ZIF-8, TSO, and ZIF-8@TSO Composite

sample	S_{BET} (m^2/g)	$S_{Langmuir}$ (m^2/g)	V_{total} (cm^3/g)[a]	D_{pore} (nm)[b]
TSO	180	190	0.54	1.3/3−20
ZIF-8	1720	1800	0.74	1.2/4
ZIF-8@TSO	400	530	0.35	1.2/4−10

[a]V_{total} (Gurvich method) was measured at P/P^0 = 0.99. [b]Micropore characteristics were calculated using the Satio and Foley method, while those for mesopores were calculated using the Barrett−Joyner−Halenda (BJH) method.

on anatase TiO_2.[63] Methoxy and methyl groups are first formed by breaking of the O−H and C−O bonds, respectively. Then, the methoxy groups are adsorbed at both Ti^{4+} ions and oxygen vacancy sites. Simultaneously, the methyl groups are adsorbed at the bridging oxygen atoms. The dissociative methanol adsorption results in a very low methanol uptake for P/P^0 ranging from 0 to 0.45. Above $P/P^0 \approx 0.45$, the molecular adsorption of methanol occurs at both Ti^{4+} ions and the surface bridging oxygen atoms via coordination and hydrogen bonding, respectively.[64,65] Hereafter, the adsorbed methanol molecules attract more methanol molecules through hydrogen bonds, leading to a capillary condensation within the mesopores. This causes the increasing uptake observed in the methanol adsorption isotherm. For ethanol, similarly, a dissociative adsorption is favored over molecular adsorption in the low pressure range, and a small capillary condensation occurs at high pressures (see Figure 7c). A typical type IV adsorption isotherm with a low ethanol uptake is observed for TSO, indicating the presence of mesopores.[27]

Interestingly, the ZIF-8@TSO composite displays a methanol adsorption isotherm with two steps, indicating it has a hierarchical porous structure (see Figure 7b). In the initial pressure range (up to P/P^0 = 0.2), the methanol uptake is negligible, mainly due to the presence of the hydrophobic ZIF-8 layer. Then, the methanol uptake increases until it reaches the first equilibrium stage (P/P^0 = 0.2−0.45), corresponding to the micropores filling of the ZIF-8. A second methanol adsorption step occurs above $P/P^0 \approx 0.45$, indicating that the methanol molecules start to fill in the mesopores of the TSO support as well as the interstitial voids between the ZIF-8 layer and the TSO support, ultimately leading to capillary condensation. Because the methanol molecular adsorption is more favorable than the dissociative adsorption on TSO above $P/P^0 \approx 0.45$, the mesopores filling plays a key role in the pressure range P/P^0 = 0.45 to 0.99. The methanol uptake for the composite is about 5.2 mmol/g at $P/P^0 \approx 0.99$, which is 50% as compared to ZIF-8 but using only 25% wt of ZIF-8.

The shape of the ethanol adsorption isotherm of the ZIF-8@TSO composite is similar to that of ZIF-8 but with a wider initial adsorption plateau (see Figure 7c). This is caused by the synergistic effect between the hydrophobic ZIF-8 layer and the TSO support, the latter facilitating a dissociative ethanol adsorption. The ethanol uptake in the ZIF8@TSO composite is only 25% of the uptake observed for ZIF-8. It indicates that the 25% wt ZIF-8 in composite plays a leading role in the ethanol adsorption, while the TSO support shows almost no ethanol adsorption across the whole pressure range.

As discussed above, the ZIF-8@TSO composite presents different adsorption properties in the presence of water, methanol, and ethanol. To gain more insight into these properties, we simulated the separation factors between ethanol and two types of contaminants, e.g., water and methanol, using the ideal adsorbed solution theory (IAST) method. Using an equimolar mixture of methanol−ethanol at 303 K, the ZIF-8@TSO composite adsorbs selectively methanol over ethanol, and the adsorption selectivity is in the range of 1.5−3.8 (see Figure 8). The increasing adsorption selectivity in the low pressure range (0−2 KPa) is caused by the methanol uptake of the ZIF-8@TSO composite which

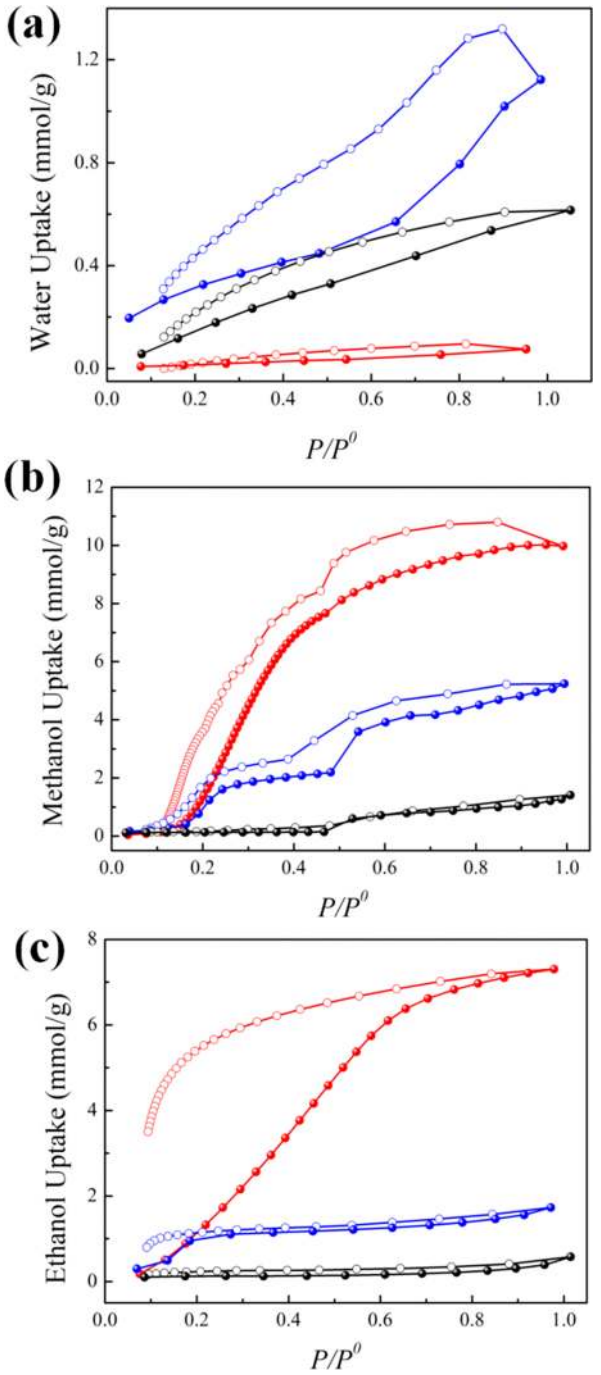

Figure 7. (a) Water, (b) methanol, and (c) ethanol adsorption isotherms for as-synthesized ZIF-8 (red), TSO support (black), and ZIF-8@TSO composite (blue) at 303 K, respectively. P^0 is the saturated pressure of the adsorbates at 303 K, which is 4 KPa, 10 KPa, and 21 KPa for water, ethanol, and methanol, respectively.

DOI: 10.1021/acsami.9b02325
ACS Appl. Mater. Interfaces 2019, 11, 21126−21136

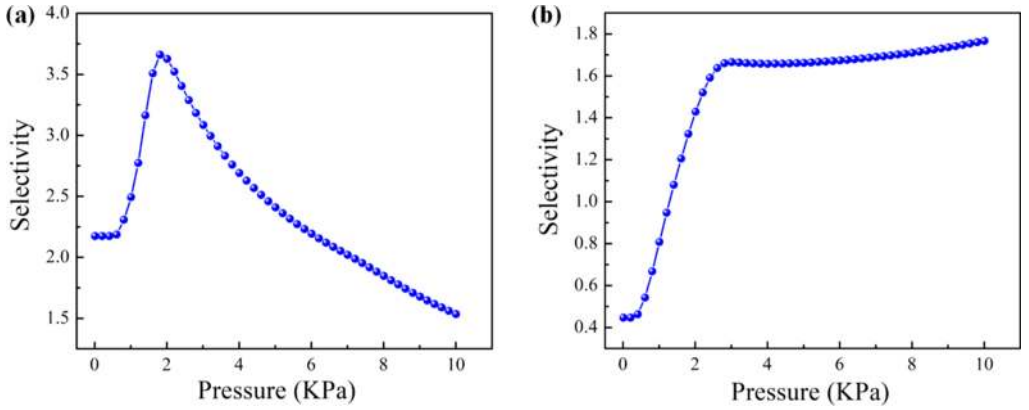

Figure 8. Adsorption selectivities calculated with the IAST method for equimolar binary mixtures of (a) methanol−ethanol and (b) ethanol−water for the ZIF-8@TSO composite at 303 K.

increases faster than the ethanol uptake. For an equimolar mixture of ethanol−water at 303 K, the ZIF-8@TSO composite adsorbs selectively water over ethanol in the pressure range of 0−2 KPa, while the ethanol is adsorbed selectively over water in the pressure range of 2−10 KPa (see Figure 8). This is also supported by the S-shape of the ethanol adsorption isotherm of the ZIF-8@TSO composite which indicates that the ethanol uptake is lower than the water uptake in the low pressure range and vice versa in the high pressure range.[66]

The separation factors of both ZIF-8 and the TSO support were also calculated by IAST simulation (see Figure S17 in the SI). Compared with the TSO support, the ZIF-8@TSO composite shows better performance for methanol−ethanol and ethanol−water mixtures. We attribute this behavior to the hierarchical porous structure of the composites and its higher surface area. Separating ethanol−water mixtures using the ZIF-8@TSO composite is less efficient as compared with ZIF-8. This is likely due to the higher surface area of ZIF-8 as compared with the ZIF-8@TSO. Moreover, ZIF-8 is much more hydrophobic than the ZIF-8@TSO composite and therefore has a lower water uptake. For an equimolar mixture of ethanol−methanol, the ZIF-8@TSO composite shows a reversed adsorption, preferring methanol over ethanol, opposite to the behavior observed for ZIF-8. The difference between methanol and ethanol uptake when using the ZIF-8@TSO composite is larger than that of the ZIF-8, likely due to the hierarchical porous structure of the ZIF-8@TSO composite.

4. CONCLUSIONS

A mixed-metal oxide material (TSO) with a hierarchical porous structure was synthesized using a sol−gel method in which natural *Populus nigra* leaves were used as a template. This mixed-oxide artificial leaf was then used as a support for growing a homogeneously dispersed ZIF-8 layer. The resulting ZIF-8@TSO composite has a hierarchical porous structure which facilitates a high methanol uptake. Using IAST simulations and an equimolar ethanol−methanol mixture, we demonstrated that the ZIF-8@TSO composite adsorbs methanol highly selectively in the low pressure range. Moreover, the ZIF-8@TSO composite is also effective in separating water−ethanol mixtures. In this case, ethanol is adsorbed selectively in the low pressure range, while water is adsorbed selectively at high pressures. This work highlights that supporting MOFs on hierarchical porous substrates not only provides a new methodology for processing MOF but also leads to unique adsorption properties of the designed materials.

■ ASSOCIATED CONTENT

Supporting Information

The Supporting Information is available free of charge on the ACS Publications website at DOI: 10.1021/acsami.9b02325.

TEM and SEM images, EDS spectra, EDS mapping, FTIR spectra, detailed adsorption isotherms, and IAST simulations (PDF)

■ AUTHOR INFORMATION

Corresponding Author

*E-mail: s.grecea@uva.nl.

ORCID

David Dubbeldam: 0000-0002-4382-1509

Stefania Tanase: 0000-0003-2830-1924

Notes

The authors declare no competing financial interest.

■ ACKNOWLEDGMENTS

Y.T. acknowledges the China Scholarship Council (CSC) for a Ph.D. fellowship. Prof. Wesley R. Browne (University of Groningen) is kindly acknowledged for the Raman spectra. This work is part of the Research Priority Area Sustainable Chemistry of the University of Amsterdam, http://suschem.uva.nl.

■ REFERENCES

(1) Sun, M. H.; Huang, S. Z.; Chen, L. H.; Li, Y.; Yang, X. Y.; Yuan, Z. Y.; Su, B. L. Application of Hierarchically Structured Porous Materials from Energy Storage and Conversion, Catalysis, Photocatalysis, Adsorption, Separation, and Sensing to Biomedicine. *Chem. Soc. Rev.* **2016**, *45*, 3479−3563.

(2) Yang, X. Y.; Chen, L. H.; Li, Y.; Rooke, J. C.; Sanchez, C.; Su, B. L. Hierarchically Porous Materials: Synthesis Strategies and Structure Design. *Chem. Soc. Rev.* **2017**, *46*, 481−588.

(3) Sun, J. K.; Xu, Q. Functional Materials Derived from Open Framework Templates/Precursors: Synthesis and Applications. *Energy Environ. Sci.* **2014**, *7*, 2071−2100.

(4) Lee, K. B.; Beaver, M. G.; Caram, H. S.; Sircar, S. Reversible Chemisorbents for Carbon Dioxide and Their Potential Applications. *Ind. Eng. Chem. Res.* **2008**, *47*, 8048−8062.

DOI: 10.1021/acsami.9b02325
ACS Appl. Mater. Interfaces 2019, 11, 21126−21136

(5) Yang, Y.; Bai, P.; Guo, X. Separation of Xylene Isotherms: A Review of Recent Advances in Materials. *Ind. Eng. Chem. Res.* **2017**, *56*, 14725−14753.
(6) He, Y.; Zhou, W.; Qian, G.; Chen, B. Methane Storage in Metal-Organic Frameworks. *Chem. Soc. Rev.* **2014**, *43*, 5657−5678.
(7) Sevilla, M.; Mokaya, R. Energy Storage Applications of Activated Carbons: Supercapacitors and Hydrogen Storage. *Energy Environ. Sci.* **2014**, *7*, 1250−1280.
(8) Das, R.; Vecitis, C. D.; Schulze, A.; Cao, B.; Ismail, A. F.; Lu, X.; Chen, J.; Ramakrishna, S. Recent Advances in Nanomaterials for Water Protection and Monitoring. *Chem. Soc. Rev.* **2017**, *46*, 6946−7020.
(9) Zhang, Y.; Yuan, S.; Feng, X.; Li, H.; Zhou, J.; Wang, B. Preparation of Nanofibrous Metal-Organic Framework Filters for Efficient Air Pollution Control. *J. Am. Chem. Soc.* **2016**, *138*, 5785−5788.
(10) Zhou, H. C.; Kitagawa, S. Metal-Organic Frameworks (MOFs). *Chem. Soc. Rev.* **2014**, *43*, 5415−5418.
(11) Vellingiri, K.; Deep, A.; Kim, K. H. Metal-Organic Frameworks as Potential Platform for Selective Treatment of Gaseous Sulfur Compounds. *ACS Appl. Mater. Interfaces* **2016**, *8*, 29835−29857.
(12) Yu, J.; Xie, L. H.; Li, J. R.; Ma, Y.; Seminario, J. M.; Balbuena, P. B. CO_2 Capture and Separations Using MOFs: Computational and Experimental Studies. *Chem. Rev.* **2017**, *117*, 9674−9754.
(13) Burtch, N. C.; Jasuja, H.; Walton, K. S. Water Stability and Adsorption in Metal-Organic Frameworks. *Chem. Rev.* **2014**, *114*, 10575−10612.
(14) Lee, J. Y.; Olson, D. H.; Pan, L.; Emge, T. J.; Li, J. Microporous Metal-Organic Frameworks with High Gas Adsorption and Separation Capacity. *Adv. Funct. Mater.* **2007**, *17*, 1255−1262.
(15) Ren, J.; Musyoka, N. M.; Langmi, H. W.; Swartbooi, A.; North, B. C.; Mathe, M. A More Efficient Way to Shape Metal-Organic Framework (MOF) Powder Materials for Hydrogen Storage Applications. *Int. J. Hydrogen Energy* **2015**, *40*, 4617−4622.
(16) Xu, C.; Yang, J.; Veenstra, M.; Sudik, A.; Purewal, J. J.; Ming, Y.; Hardy, B. J.; Warner, J.; Maurer, S.; Mueller, U.; Siegel, D. J. Hydrogen Permeation and Diffusion in Densified MOF-5 pellets. *Int. J. Hydrogen Energy* **2013**, *38*, 3268−3274.
(17) Ren, J. W.; Langmi, H. W.; North, B. C.; Mathe, M. Review on Processing of Metal-Organic Framework (MOF) Materials towards System Integration for Hydrogen Storage. *Int. J. Energy Res.* **2015**, *39*, 607−620.
(18) Chen, Y.; Huang, X.; Zhang, S.; Li, S.; Cao, S.; Pei, X.; Zhou, J.; Feng, X.; Wang, B. Shaping of Metal-Organic Frameworks: from Fluid to Shaped Bodies and Robust Foams. *J. Am. Chem. Soc.* **2016**, *138*, 10810−10813.
(19) Liang, X. Q.; Zhang, F.; Feng, W.; Zou, X. Q.; Zhao, C. J.; Na, H.; Liu, C.; Sun, F. X.; Zhu, G. S. From Metal-Organic Framework (MOF) to MOF-Polymer Composite Membrane: Enhancement of Low-Humidity Proton Conductivity. *Chem. Sci.* **2013**, *4*, 983−992.
(20) Lin, R.; Ge, L.; Diao, H.; Rudolph, V.; Zhu, Z. H. Ionic Liquids as the MOFs/Polymer Interfacial Binder for Efficient Membrane Separation. *ACS Appl. Mater. Interfaces* **2016**, *8*, 32041−32049.
(21) Shah, M.; McCarthy, M. C.; Sachdeva, S.; Lee, A. K.; Jeong, H. K. Current Status of Metal-Organic Framework Membranes for Gas Separations: Promises and Challenges. *Ind. Eng. Chem. Res.* **2012**, *51*, 2179−2199.
(22) Caro, J. Hierarchy in Inorganic Membranes. *Chem. Soc. Rev.* **2016**, *45*, 3468−3478.
(23) Li, X. F.; Fan, T. X.; Zhou, H.; Chow, S. K.; Zhang, W.; Zhang, D.; Guo, Q. X.; Ogawa, H. Enhanced Light-Harvesting and Photocatalytic Properties in Morph-TiO_2 from Green-Leaf Biotemplates. *Adv. Funct. Mater.* **2009**, *19*, 45−46.
(24) Solomon, B. R.; Hyder, M. N.; Varanasi, K. K. Separating Oil-Water Nanomulsions using Flux-Enhanced Hierarchical Membranes. *Sci. Rep.* **2015**, *4*, 5504.
(25) Liu, J.; Yang, Q.; Wang, W. T.; Li, M. Z.; Song, Y. L. Aquatic Plant Inspired Hierarchical Artificial Leaves for Highly Efficient Photocatalysis. *J. Mater. Chem. A* **2013**, *1*, 7760−7766.
(26) Luque, R.; Herrero-Davila, L.; Campelo, J. M.; Clark, J. H.; Hidalgo, J. M.; Luna, D.; Marinas, J. M.; Romero, A. A. Biofuels: A Technological Perspective. *Energy Environ. Sci.* **2008**, *1*, 542−564.
(27) Zhang, K.; Lively, R. P.; Zhang, C.; Koros, W. J.; Chance, R. R. Investigating the Intrinsic Ethanol/Water Separation Capability of ZIF-8: An Adsorption and Diffusion Study. *J. Phys. Chem. C* **2013**, *117*, 7214−7225.
(28) Bourrelly, S.; Moulin, B.; Rivera, A.; Maurin, G.; Devautour-Vinot, S.; Serre, C.; Devic, T.; Horcajada, P.; Vimont, A.; Clet, G.; Daturi, M.; Lavalley, J.-C.; Loera-Serna, S.; Denoyel, R.; Llewellyn, P. L.; Ferey, G. Explanation of Adsorption of Polar Vapors in the Highly Flexible Metal Organic Framework MIL-53 (Cr). *J. Am. Chem. Soc.* **2010**, *132*, 9488−9498.
(29) Borjigin, T.; Sun, F. X.; Zhang, J. L.; Cai, K.; Ren, K.; Zhu, G. S. A Microporous Metal-Organic Framework with High Stability for GC Separation of Alcohols from Water. *Chem. Commun.* **2012**, *48*, 7613−7615.
(30) Lin, Z. J.; Zou, R. Q.; Liang, J.; Xia, W.; Xia, D. G.; Wang, Y. X.; Lin, J. H.; Hu, T. L.; Chen, Q.; Wang, X. D.; Zhao, Y. S.; Burrell, A. K. Pore Size-Controlled Gases and Alcohols Separation with Ultramicroporous Homochiral Lanthanide-Organic Frameworks. *J. Mater. Chem.* **2012**, *22*, 7813−7818.
(31) Shigematsu, A.; Yamada, T.; Kitagawa, H. Selective Separation of Water, Methanol, and Ethanol by a Porous Coordination Polymer Built with a Flexible Tetrahedral Ligand. *J. Am. Chem. Soc.* **2012**, *134*, 13145−13147.
(32) Cravillon, J.; Nayuk, R.; Springer, S.; Feldhoff, A.; Huber, K.; Wiebcke, M. Controlling Zeolitic Imidazolate Framework Nano-and Microcrystal Formation: Insight into Crystal Growth by Time-Resolved *in situ* Static Light Scattering. *Chem. Mater.* **2011**, *23*, 2130−2141.
(33) Grosu, Y.; Renaudin, G.; Eroshenko, V.; Nedelec, J.-M.; Grolier, J.-P. E. Synergetic Effect of Temperature and Pressure on Energetic and Structural Characteristics of {ZIF-8+ Water} Molecular Spring. *Nanoscale* **2015**, *7*, 8803−8810.
(34) Shi, G. M.; Yang, T.; Chung, T. S. Polybenzimidazole (PBI)/Zeolitic Imidazolate Frameworks (ZIF-8) Mixed Matrix Membranes for Pervaporation Dehydration of Alcohols. *J. Membr. Sci.* **2012**, *415−416*, 577−586.
(35) Liu, S.; Liu, G.; Zhao, X.; Jin, W. Hydrophobic-ZIF-71 Filled PEBA Mixed Matrix Membranes for Recovery of Biobutanol via Pervaporation. *J. Membr. Sci.* **2013**, *446*, 181−188.
(36) Li, Y.; Wee, L. H.; Martens, J. A.; Vankelecom, F. J. ZIF-71 as a Potential Filler to Prepare Pervaporation Membranes for Bio-Alcohol Recovery. *J. Mater. Chem. A* **2014**, *2*, 10034−10040.
(37) Li, Q.; Liu, Q.; Zhao, J.; Hua, Y.; Sun, J.; Duan, J.; Jin, W. High Efficient Water/Ethanol Separation by a Mixed Matrix Membrane Incorporating MOF Filler with High Water Adsorption Capacity. *J. Membr. Sci.* **2017**, *544*, 68−78.
(38) Mao, H.; Zhen, H.-G.; Ahmad, A.; Zhang, A.-S.; Zhao, Z.-P. *In situ* Fabrication of MOF Nanoparticles in PDMS Membrane *via* Interfacial Synthesis for Enhanced Ethanol Permselective Pervaporation. *J. Membr. Sci.* **2019**, *573*, 344−358.
(39) Kang, C.-H.; Lin, Y.-F.; Huang, Y.-S.; Tung, K.-L.; Chang, K.-S.; Chen, J.-T.; Hung, W.-S.; Lee, K.-R.; Lai, J.-Y. Synthesis of ZIF-7/Chitosan Mixed-Matrix Membranes with Improved Separation Performance of Water/Ethanol Mixtures. *J. Membr. Sci.* **2013**, *438*, 105−111.
(40) Plessius, R.; Kromhout, R.; Ramos, A. L. D.; Ferbinteanu, M.; Mittelmeijer-Hazeleger, M. C.; Krishna, R.; Rothenberg, G.; Tanase, S. Highly Selective Water Adsorption in a Lanthanum Metal-Organic Framework. *Chem. - Eur. J.* **2014**, *20*, 7922−7925.
(41) Zhou, H.; Guo, J. J.; Li, P.; Fan, T. X.; Zhang, D.; Ye, J. H. Leaf-Architectured 3D Hierarchical Artificial Photosynthetic System of Perovskite Titanates towards CO_2 Photoreduction into Hydrocarbon Fuels. *Sci. Rep.* **2013**, *3*, 1667.
(42) Zhou, H.; Li, X. F.; Fan, T. X.; Osterloh, F. E.; Ding, J.; Sabio, E. M.; Zhang, D.; Guo, Q. Artificial Inorganic Leafs for Efficient

DOI: 10.1021/acsami.9b02325
ACS Appl. Mater. Interfaces 2019, 11, 21126−21136

Photochemical Hydrogen Production Inspired by Natural Photosynthesis. *Adv. Mater.* **2010**, *22*, 951−956.
(43) Li, J.; Hoffmann, M. W. G.; Shen, H.; Fabrega, C.; Prades, J. D.; Andreu, T.; Hernandez-Ramirez, F.; Mathur, S. Enhanced Photoelectrochemical Activity of an Excitonic Staircase in CdS@TiO_2 and CdS@Anatase@Rutile TiO_2 Heterostructures. *J. Mater. Chem.* **2012**, *22*, 20472−20476.
(44) Jiang, J.; Tang, X.; Zhou, S.; Ding, J.; Zhou, H.; Zhang, F.; Zhang, D.; Fan, T. Synthesis of Visible and Near Infrared Light Sensitive Amorphous Titania for Photocatalytic Hydrogen Evolution. *Green Chem.* **2016**, *18*, 2056−2062.
(45) Abad, J.; Gonzalez, C.; Andres, P. L.; Roman, E. Characterization of Thin Silicon Overlayers on Rutile TiO_2(101)-(1 × 1). *Phys. Rev. B: Condens. Matter Mater. Phys.* **2010**, *82*, 165420.
(46) Shi, N.; Li, X.; Fan, T.; Zhou, H.; Ding, J.; Zhu, H. Biogenic N-I-Codoped TiO_2 Photocatalyst Derived from *kelp* for Efficient Dye Degradation. *Energy Environ. Sci.* **2011**, *4*, 172−180.
(47) Xin, X.; Xu, T.; Yin, J.; Wang, L.; Wang, C. Management on the Location and Concentration of Ti^{3+} in Anatase TiO_2 for Defects-Induced Visible-Light Photocatalysis. *Appl. Catal., B* **2015**, *176*, 354−362.
(48) Lin, L.; Zhang, T.; Zhang, X.; Liu, H.; Yeung, K.; Qiu, J. New Pd/SiO2@ZIF-8 core-shell catalyst with selective, antipoisoning, and antileaching properties for the hydrogenation of alkenes. *Ind. Eng. Chem. Res.* **2014**, *53*, 10906−10913.
(49) Zhang, T.; Zhang, X.; Yan, X.; Kong, L.; Zhang, G.; Liu, H.; Qiu, J.; Yeung, K. L. Synthesis of Fe_3O_4@ZIF-8 Magnetic Core-Shell Microspheres and Their Potential Application in a Capillary Microreactor. *Chem. Eng. J.* **2013**, *228*, 398−404.
(50) Hu, Y.; Li, C.; Gu, F.; Zhao, Y. Facile Flame Synthesis and Photoluminescent Properties of Core/Shell TiO_2/SiO_2 Nanoparticles. *J. Alloys Compd.* **2007**, *432*, L5−L9.
(51) Sun, H.; Tang, B.; Wu, P. Two-Dimensional Zeolitic Imidazolate Framework/Carbon Nanotube Hybrid Networks Modified Proton Exchange Membranes for Improving Transport Properties. *ACS Appl. Mater. Interfaces* **2017**, *9*, 35075−35085.
(52) Kaur, H.; Mohanta, G. C.; Gupta, V.; Kukkar, D.; Tyagi, S. Synthesis and Characterization of ZIF-8 Nanoparticles for Controlled Release of 6-Mercaptopurine Drug. *J. Drug Delivery Sci. Technol.* **2017**, *41*, 106−112.
(53) Fu, Y. Y.; Yang, C. X.; Yan, X. P. Fabrication of ZIF-8@SiO_2 Core-Shell Microspheres as the Stationary Phase for High-Performance Liquid Chromatography. *Chem. - Eur. J.* **2013**, *19*, 13484−13491.
(54) Liu, X. L.; Li, Y. S.; Ban, Y. J.; Peng, Y.; Jin, H.; Bux, H.; Xu, L. Y.; Caro, J.; Yang, W. S. Improvement of Hydrothermal Stability of Zeolitic Imidazolate Frameworks. *Chem. Commun.* **2013**, *49*, 9140−9142.
(55) Zhang, L. W.; Fu, H. B.; Zhu, Y. F. Efficient TiO_2 Photocatalysts from Surface Hydbridization of TiO_2 Particles with Graphite-like Carbon. *Adv. Funct. Mater.* **2008**, *18*, 2180−2189.
(56) Chakraborty, A.; Achari, A.; Eswaramoorthy, M.; Maji, T. K. MOF-Aminoclay Composites for Superior CO_2 Capture, Separation and Enhanced Catalytic Activity in Chemical Fixation of CO_2. *Chem. Commun.* **2016**, *52*, 11378−11381.
(57) Zhang, K.; Lively, R. P.; Dose, M. E.; Brown, A. J.; Zhang, C.; Chung, J.; Nair, S.; Koros, W. J.; Chance, R. R. Alcohol and Water Adsorption in Zeolitic Imidazolate Frameworks. *Chem. Commun.* **2013**, *49*, 3245−3247.
(58) Yang, H. G.; Sun, C. H.; Qiao, S. Z.; Zou, J.; Liu, G.; Smith, S. C.; Cheng, H. M.; Lu, G. Q. Anatase TiO_2 Single Crystals with a Large Percentage of Reactive Facets. *Nature* **2008**, *453*, 638−641.
(59) Hair, M. L. Hydroxyl Groups on Silica Surface. *J. Non-Cryst. Solids* **1975**, *19*, 299−309.
(60) de Lange, M. F.; van Velzen, B. L.; Ottevanger, C. P.; Verouden, K. J. F. M.; Lin, L. C.; Vlugt, T. J. H.; Gascon, J.; Kapteijn, F. Metal-Organic Frameworks in Adsorption-Driven Heat Pumps: the Potential of Alcohols as Working Fluids. *Langmuir* **2015**, *31*, 12783−12796.
(61) Nalaparaju, A.; Zhao, X. S.; Jiang, J. W. Molecular Understanding for the Adsorption of Water and Alcohols in Hydrophilic and Hydrophobic Zeolitic Metal-Organic Frameworks. *J. Phys. Chem. C* **2010**, *114*, 11542−11550.
(62) Herman, G. S.; Dohnalek, Z.; Ruzycki, N.; Diebold, U. Experimental Investigation of the Interaction of Water and Methanol with Anatase TiO_2 (101). *J. Phys. Chem. B* **2003**, *107*, 2788−2795.
(63) Zhang, Z.; Bondarchuk, O.; White, J. M.; Kay, B. D.; Dohnalek, Z. Imaging Adsorbate O-H Bond Cleavage: Methanol on TiO_2(110). *J. Am. Chem. Soc.* **2006**, *128*, 4198−4199.
(64) Wang, C.; Groenzin, H.; Shultz, M. J. Direct Observation of Competitive Adsorption between Methanol and Water on TiO_2: an *in situ* Sum-Frequency Generation Study. *J. Am. Chem. Soc.* **2004**, *126*, 8094−8095.
(65) Carrizosa, I.; Munuera, G. Study of the Interaction of Aliphatic Alcohols with TiO_2. *J. Catal.* **1977**, *49*, 174−188.
(66) Challa, S. R.; Sholl, D. S.; Johnson, J. K. Adsorption and Separation of Hydrogen Isotopes in Carbon Nanotubes: Multicomponent Grand Canonical Monte Carlo Simulations. *J. Chem. Phys.* **2002**, *116*, 814−824.

DOI: 10.1021/acsami.9b02325
ACS Appl. Mater. Interfaces 2019, 11, 21126−21136